



CHORUS

This is the accepted manuscript made available via CHORUS. The article has been published as:

Magnetic and spin-orbit exciton excitations in the
honeycomb lattice compound RuBr_3

Youngsu Choi, Je-Ho Lee, Seungyeol Lee, Dirk Wulferding, Hideyuki Fujihara, Fuki Sato,
Yoshinori Imai, Kenya Ohgushi, Maeng-Je Seong, and Kwang-Yong Choi

Phys. Rev. B **106**, 174430 — Published 22 November 2022

DOI: [10.1103/PhysRevB.106.174430](https://doi.org/10.1103/PhysRevB.106.174430)

Magnetic and spin-orbit exciton excitations in the honeycomb lattice RuBr₃

Youngsu Choi,¹ Je-Ho Lee,² Seungyeol Lee,³ Dirk Wulferding,^{4,5} Hideyuki Fujihara,⁶ Fuki Sato,⁶ Yoshinori Imai,⁶ Kenya Ohgushi,⁶ Maeng-Je Seong,^{2,*} and Kwang-Yong Choi^{3,†}

¹*Department of Energy Science, Sungkyunkwan University, Suwon 16419, Republic of Korea*

²*Department of Physics, Chung-Ang University, Seoul 06974, Republic of Korea*

³*Department of Physics, Sungkyunkwan University, Suwon 16419, Republic of Korea*

⁴*Center for Correlated Electron Systems, Institute for Basic Science, Seoul 08826, Republic of Korea*

⁵*Department of Physics and Astronomy, Seoul National University, Seoul 08826, Republic of Korea*

⁶*Department of Physics, Graduate School of Science, Tohoku University,*

6-3 Aramaki-Aoba, Aoba-ku, Sendai, Miyagi 980-8578, Japan

(Dated: November 10, 2022)

RuX₃ trihalides (X =halogen atoms) offer a prominent platform for exploring the Kitaev spin liquid. Using polarization-resolved Raman spectroscopy, we report a comparative study of lattice, magnetic, and electronic excitations on X =Cl and Br. Our phonon Raman spectra show that RuBr₃ retains a three-layer honeycomb lattice without structural transition, unlike α -RuCl₃ that undergoes a monoclinic-to-rhombohedral structural transition at ~ 150 K. In addition, both RuX₃ compounds commonly feature single and double spin-orbit excitons of almost identical energies, alluding to the realization of a $j_{\text{eff}} = 1/2$ state to the same degree. In contrast to α -RuCl₃ two-magnon scattering dominates over fractionalized excitations in RuBr₃. Our results suggest that a Br-for-Cl substitution moves RuX₃ further away from a pure Kitaev phase despite enhanced $p-d$ hybridization.

PACS numbers: 75.10.Pq, 75.50.Ee

I. INTRODUCTION

Over the last decades, the theoretical proposal of a Z_2 quantum spin liquid (QSL) in the $S = 1/2$ Kitaev honeycomb model has sparked experimental endeavors to substantialize QSLs in $4d$ and $5d$ Mott insulators with strong spin-orbit coupling (SOC) [1–9]. Singularly, a Kitaev QSL harbors a variety of exotic elementary excitations, including itinerant Majorana fermions and localized fluxes at zero field as well as anyons with non-Abelian statistics and chiral Majorana edge modes in the presence of a small external magnetic field [1, 10, 11]. The latter has strong relevance to fault-tolerant quantum computation.

In the quest for Majorana fermions in a magnetic insulator, RuX₃ trihalides (X =Cl, Br, I) have been extensively investigated as benchmark materials [12–16]. α -RuCl₃ shows zigzag magnetic order at $T_N \approx 7$ K, precluding a Kitaev QSL. Although the long-range magnetic order and trigonal lattice distortions conceal inherent Kitaev physics, there is ample experimental and theoretical evidence that α -RuCl₃ lies close to a Kitaev phase boundary [17–24]. These tantalizing signatures for Kitaev magnetism give impetus to tuning selectively the strength of Kitaev, Heisenberg, Γ , and Γ' interactions towards achieving a sought-after Kitaev QSL. One promising approach is to control $p-d$ hybridization, SOC, and electron correlations by halogen substitution. At ambient pressure, however, only polymorphs with a one-dimensional chain structure (space group:

$P6_3/mcm$) have been known, which form a Ru dimerized state [12–14]. We recall that the molecular orbital state formed in chain polymorphs quenches spin-orbital-entangled $j_{\text{eff}} = 1/2$ degrees of freedom.

In this stalemate, honeycomb polymorphs of RuX₃ were recently synthesized under moderately high pressures [25–27]. RuBr₃ turns out to share common electronic and magnetic properties with its sibling α -RuCl₃, namely, a spin-orbit-assisted Mott insulator and zigzag magnetic order, except that the Néel temperature increases up to $T_N \approx 34$ K. In sharp contrast, RuI₃ shows metallic and paramagnetic behaviors with no indication of long-range magnetic order down to 0.35 K.

Subsequent first-principles calculations [28–30] uncover that the nearest-neighbor (NN) hopping parameters are suppressed with increasing ligand atomic number in spite of the stronger hybridization. On the other hand, further-neighbor magnetic exchange parameters are enhanced in gross. This intriguing tendency implies the increasingly significant role of further-neighbor exchange interactions in determining a ground state, going from Cl to Br to I. As to honeycomb RuI₃, the resistivity data are typical for semimetallic behavior, yet the theoretical calculations disagree on conducting properties. Kaib *et al.* [29] purported that RuI₃ is on the insulating side of a metal-insulator transition. Conversely, Zhang *et al.* [30] spoke for the metallicity arising from the reduction of electronic correlation due to the strong hybridization between Ru $4d$ and I $5p$ orbitals.

To assess the viability of Kitaev magnetism in the RuX₃ family, it is highly desired to probe directly low-energy electronic and magnetic excitations. In the previous works of α -RuCl₃ [31–42], Raman spectroscopy was well-established as an experimental tool for gauging Ki-

* Corresponding author: mseong@cau.ac.kr

† Corresponding author: choisky99@skku.edu

taev and non-Kitaev interaction, crystal structure, SOC, and Mottness in extended Kitaev systems.

In this study, we employ polarization-resolved Raman spectroscopy to characterize phonon, magnetic, and electronic excitations of RuX_3 ($X=\text{Cl}, \text{Br}$) with respect to temperature, symmetry, and dynamics. A detailed comparison of RuX_3 unravels that RuBr_3 moves away from the much-wanted Kitaev realm, possibly due to enlarged further-neighbor exchange interactions, compared to $\alpha\text{-RuCl}_3$.

II. EXPERIMENTAL DETAILS

Single crystals of $\alpha\text{-RuCl}_3$ were grown by a vacuum sublimation method [24]. X-ray and neutron diffraction investigations of $\alpha\text{-RuCl}_3$ showed that a structural transition occurs from the room-temperature monoclinic ($C2/m$) to the low-temperature rhombohedral ($R\bar{3}$) structure [43]. Polycrystalline samples of RuBr_3 with a honeycomb lattice were synthesized using a cubic-anvil high-pressure apparatus as detailed in Ref. [25].

For the Raman scattering experiment, the samples were installed into a He closed-cycle cryostat with a varying temperature range of $T=3\text{-}300$ K. The scattered light was collected with a single-grating spectrometer (Princeton Instruments, SP-2500i) equipped with a liquid-nitrogen-cooled CCD (charge-coupled device) detector. We collected the Raman spectra in an exact backscattering geometry with the laser excitation line $\lambda=532$ nm. A Bragg notch filter (BNF) was used for spectral narrowing of the incident light. Rayleigh scattering was substantially eliminated by using additional BNFs, enabling the observation of a Raman signal down to ~ 15 cm^{-1} .

III. RESULTS

A. Phonon Raman spectra

As the detailed Raman spectra of $\alpha\text{-RuCl}_3$ were reported in the previous works [31–39], a comparative Raman study of honeycomb polymorphs RuX_3 ($X=\text{Cl}, \text{Br}$) will shed light on the possible differences and similarities in their crystal structure and stacking pattern. We conducted Raman scattering measurements using a circularly polarized light that is incident and scattered on a honeycomb layer. In Kitaev-dominant honeycomb magnets, magnetic and electronic excitations are dominant in in-plane scattering channels. Thus, circularly polarized light, lying in the ab plane, is sufficient for making one-to-one comparison of Raman spectra between $\alpha\text{-RuCl}_3$ and honeycomb polymorphs RuBr_3 .

For the rhombohedral $R\bar{3}$ space group, the factor group analysis predicts a total of eight Raman-active phonon modes, $\Gamma_{\text{Raman}} = 4A_g(aa,bb,cc) + 4E_g(aa,bb,ab,ac,bc)$. Shown in Fig. 1 are the Raman spectra of $\alpha\text{-RuCl}_3$

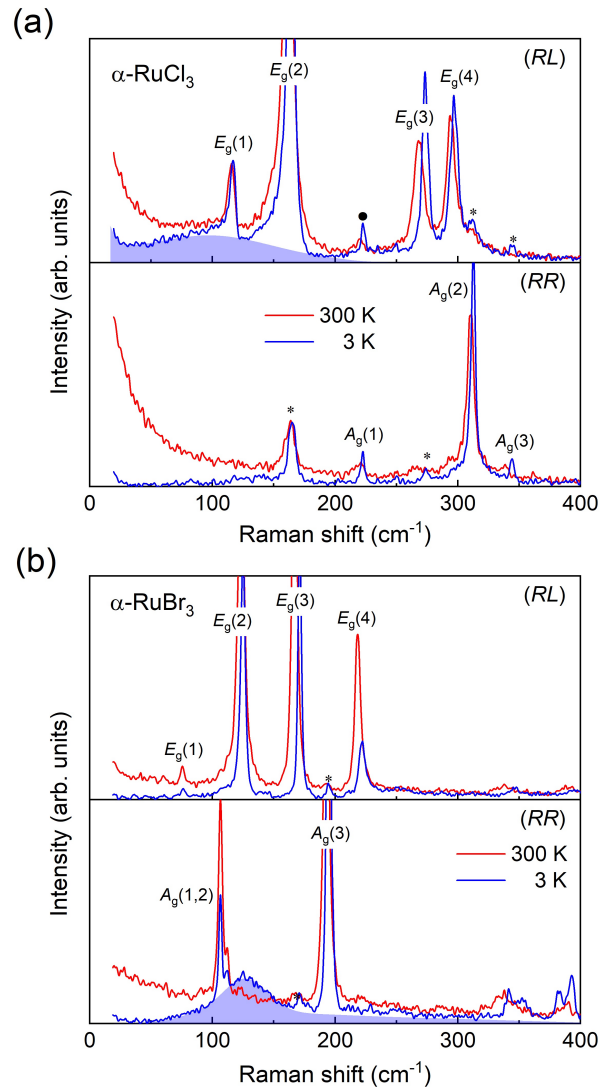


FIG. 1. Low-energy Raman spectra of (a) $\alpha\text{-RuCl}_3$ and (b) RuBr_3 measured in (RL) and (RR) polarizations at $T=300$ K (red line) and 3 K (blue line). Phonon modes are labeled according to A_g and E_g symmetry. The asterisks indicate a polarizer leakage and the black dot is an activated phonon due to reverse-observe twinning. The color shadings depict a magnetic continuum.

and RuBr_3 measured in (RL) and (RR) polarizations at $T=300$ K and 3 K. The circular (RL) and (RR) polarizations in the ab plane correspond to $aa - bb - i(ab + ba)$ and $aa + bb - i(ab - ba)$ geometries with $R = a - ib$ and $L = a + ib$, respectively, and probe selectively the respective E_g and A_g symmetry. Notably, $\alpha\text{-RuCl}_3$ undergoes the monoclinic-to-rhombohedral transition that is driven by the alteration of layer stacking sequence sequence [43]. This type of structural transition is not expected to induce an appreciable change in phonon peaks (see below for more details). Thus, the phonon assignment is made based on the low- T $R\bar{3}$ space group. We refer to Ref. [32] for the phonon assignment in terms of the high- T $C2/m$

space group.

At $T = 300$ K we identify the four E_g modes assigned as 115.6 cm^{-1} [$E_g(1)$ mode], 163.2 cm^{-1} [$E_g(2)$], 271.9 cm^{-1} [$E_g(3)$], and 295.8 cm^{-1} [$E_g(4)$], and three A_g modes as 221.6 cm^{-1} [$A_g(1)$ mode], 311 cm^{-1} [$A_g(2)$], and 343.7 cm^{-1} [$A_g(3)$] for α -RuCl₃. One A_g mode cannot be resolved due to its small scattering cross section. A close look at the phonon spectra reveals that the phonon modes are divided into two groups separated by 200 cm^{-1} . The lower-energy modes below 200 cm^{-1} involve mainly the motion of the heavier Ru atoms: twist of the Ru-Cl-Ru-Cl plane and Ru in-plane relative movement [31]. On the other hand, the higher-energy modes are dictated by the displacement of Cl atoms: Ru-Cl-Ru-Cl plane shearing, breathing motion of Ru-Cl-Ru-Cl ring, and symmetrical breathing between the upper and lower chlorine layers. On cooling down to $T = 3$ K, fine features (marked by the asterisks and dot) become visible. The asterisks are associated with a polarizer leakage, inferring from the fact that they have partner modes with the same frequency and strong scattering intensity in different polarizations. The 222 cm^{-1} peak (black dot) is ascribed to an activated phonon arising from reverse-observe twinning or stacking faults [23]. We find neither a split of peaks nor additional phonon modes through the structural transition at 150 K from the monoclinic $C2/m$ to the rhombohedral $R\bar{3}$ structure [23, 32, 33]. The weak influence of the structural symmetry reduction on the phonon spectra confirms that the alteration of the layer stacking sequence exerts little effect on lattice dynamics in van der Waals materials.

We next turn to the Raman spectra of RuBr₃ shown in Fig. 1(b). **It is remarkable that the polarized Raman spectra of single-crystalline domains obey the same polarization dependence as those of α -RuCl₃.** At $T = 300$ K, we detect the four E_g modes at 75.2 cm^{-1} [$E_g(1)$], 124.8 cm^{-1} [$E_g(2)$], 171.2 cm^{-1} [$E_g(3)$], and 221.9 cm^{-1} [$E_g(4)$], and the three A_g modes at 116.6 cm^{-1} [$A_g(1)$], 112.7 cm^{-1} [$A_g(2)$], and 194.6 cm^{-1} [$A_g(3)$]. We note that RuBr₃ and its counterpart CrBr₃ show similar phonon spectra [44]. Compared to α -RuCl₃, the phonon frequencies of α -RuBr₃ are reduced roughly by 30 %, consistent with the calculated phonon frequencies [45]. Unlike α -RuCl₃, however, the low- T spectra exhibit no additional feature related to stacking disorders, indicative of the formation of a uniform stacking pattern. This observation is in accord with the notion that a honeycomb polymorph of RuBr₃ lacks a structural phase transition and retains a three-layered honeycomb structure over the whole temperature range [25].

Before proceeding, we recall the selection rule for Majorana spinon excitations. In a pure Kitaev model, magnetic Raman scattering is exclusively permitted in the (RL) channel (E_g symmetry) [46]. In an extended Kitaev system, non-Loudon-Fleury (non-LF) scattering terms contribute to a magnetic Raman signal, thereby modifying the polarization dependence expected from the conventional LF mechanism [47]. For α -RuCl₃, a magnetic

continuum prevails in the E_g symmetry [see the color shading in the upper panel of Fig. 1(a)]. We single out the magnetic Raman response by subtracting two Fano phonons from the total Raman scattering intensity. We refer to our prior work for a fitting procedure (Fig. 4(a) in Ref. [23]). This is contrasted by RuBr₃ whose magnetic excitations are dominant in the A_g symmetry [see the color shading in the lower panel of Fig. 1(b)]. **As discussed below, the distinct selection rule of the magnetic excitation is related to the altering nature of quasiparticles. More specifically, two-magnon scattering is dominant in RuBr₃.**

B. Thermal evolution of the phonon parameters

Figure 2(a) presents the thermal evolution of the Raman spectra of RuBr₃ measured in (RR) polarization by heating from $T = 3$ K to 300 K. In the chosen (RR) scattering channel, the interference between optical phonons and magnetic scattering is minimized, while the magnetic excitations are the strongest.

At $T = 3$ K, we observe three A_g modes superimposed on a weak, broad magnetic continuum centered at 127 cm^{-1} and extending to $\sim 300 \text{ cm}^{-1}$. With increasing temperature, the magnetic continuum evolves into a quasielastic scattering due to the thermal damping of spin excitations (see below for further discussion). To trace the thermal behavior of the phonon modes, we fit them to Lorentzian profiles. The extracted phonon parameters of the $A_g(1)$ and $A_g(3)$ modes are plotted as a function of temperature in Figs. 2(b) and 2(c), respectively. Overall, the phonon frequencies show an increasing trend with decreasing temperature, while the full width at half-maximum (FWHM) decreases. To examine phonon anomalies due to spin-phonon coupling, we attempted to analyze the temperature dependence of the phonon parameters in terms of the anharmonic phonon model [48]

$$\omega(T) = \omega_0 + A[1 + 2/(e^{\hbar\omega_0/2k_B T} - 1)], \quad (1)$$

$$\Gamma(T) = \Gamma_0 + B[1 + 2/(e^{\hbar\omega_0/2k_B T} - 1)]. \quad (2)$$

Here, ω_0 and Γ_0 are the phonon frequency and linewidth at $T=0$ K, respectively, and A and B are the coefficient describing cubic anharmonic contribution to $\omega(T)$ and $\Gamma(T)$.

Upon heating, the $A_g(1)$ and $A_g(3)$ modes exhibit a weak hardening by $0.5 - 2 \text{ cm}^{-1}$, revealing deviation from the anharmonic phonon-phonon model. For the $A_g(3)$ mode, the frequency, FWHM, and normalized intensity show anomalies below $T^* \sim 70$ K. The characteristic temperature T^* corresponds to the broad maximum in the static magnetic susceptibility $\chi^{\text{stat}}(T)$ [25] [see the solid line in Fig. 3(c)]. This implies that the phonon anomalies are linked to the development of magnetic correlations. In contrast, the $A_g(1)$ mode, lying on top of the magnetic continuum, displays anomalous behavior in

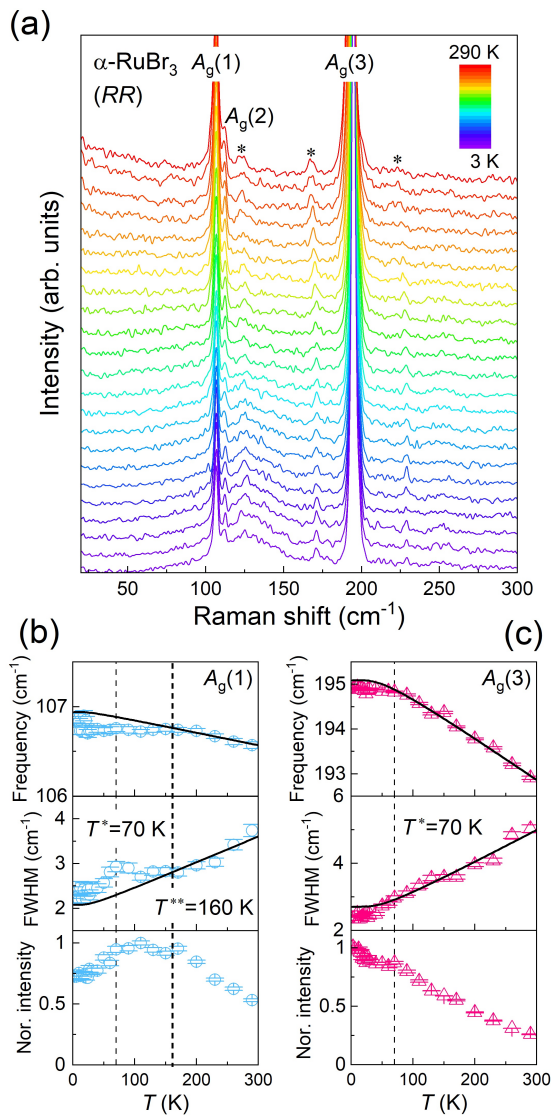


FIG. 2. (a) Temperature dependence of the Raman spectra of RuBr₃ measured in (RR) polarization. The asterisks denote a leakage of polarizer. Thermal evolution of the frequency, the FWHM, and the normalized intensity of (b) the $A_g(1)$ and (c) the $A_g(3)$ mode. The solid lines represent the anharmonic phonon interaction model as described in the text. The vertical dashed lines mark the two characteristic temperatures $T^* = 70$ K and $T^{**} = 160$ K.

a wider temperature range below $T^{**} \sim 160$ K. More specifically, the FWHM is broader than the anharmonic estimate below T^{**} , alluding to the presence of an additional decaying channel. In the identical temperature interval, the phonon frequency is shifted to lower energy than the anharmonic value. Noteworthy is that the recent theoretical calculation on optical phonons coupled to a Kitaev QSL predicts the renormalization of phonon energy and the shortening of phonon lifetime [40–42]. As such, our phonon anomalies raise the possibility of coupling the optical $A_g(1)$ phonon to the magnetic continuum that entails fractionalized quasiparticles (see the fol-

lowing subsection for detailed analysis). In this scenario, $T^{**} \sim 160$ K is linked to the onset of spin fractionalization.

C. Magnetic Raman scattering of RuBr₃

We now expound on the nature of magnetic excitations observed in the A_g $[(RR)]$ scattering channel [see the violet shading in the lower panel of Fig. 1(b)]. In Fig. 3(a), we present the thermal evolution of the magnetic Raman susceptibility $\chi''(\omega, T)$ obtained after subtracting phonon peaks from the as-measured spectra $I(\omega)$. Here, $\chi''(\omega)$ is related to $I(\omega)$ through the relation $I(\omega) = (1 + n(\omega))\chi''(\omega)$ with the Bose-factor $n(\omega) = [1 - \exp(\hbar\omega/k_B T)]^{-1}$.

With increasing temperature, the magnetic continuum systematically softens and dampens. The spectral form is approximately described by a sum of three Gaussian profiles $I_{\text{mag}}(\omega) = \sum_{i=1}^3 \frac{A_i}{\sigma_i \sqrt{2\pi}} \exp(-\frac{(\omega - \omega_i)^2}{\sigma_i^2})$. The orange shading with the fitting parameters $\omega_1 = 126.9(9)$ cm⁻¹, $\sigma_1 = 42.3(9)$ cm⁻¹, and $A_1 = 0.73$ represents two-magnon scattering (abbreviated as 2M). On the other hand, the sea-green shading the parameters $\omega_2 = 88.6(3)$ cm⁻¹, $\omega_3 = 178.6(3)$ cm⁻¹, $\sigma_2 = 30.4(5)$ cm⁻¹, $\sigma_3 = 188.7(5)$ cm⁻¹, $A_2 = 0.07$ and $A_3 = 1$ is associated with the rest magnetic excitations (abbreviated as ME). The two-component decomposition of the magnetic excitations points to the presence of two disparate quasiparticles.

We further visualize this thermal behavior in the color plot of $\chi''(\omega, T)$ vs. temperature in Fig. 3(b). The thermal softening and damping of the magnetic excitations experiences marked changes through T^* and T^{**} [see the solid and dashed lines in Fig. 3(b)]. The red-shifting of the peak energy is not compatible with the thermal characteristics of Majorana fermions, which remain unchanged with temperature [49]. Rather, this thermal behavior is highly reminiscent of the renormalization and damping of two-magnons in antiferromagnets [37, 50]. Thus, we assign the 2M contribution to two-magnon scattering which originates through double spin-flip processes by inelastic light scattering within the LF theory [51]. The broad spectral weight extending to 300 cm⁻¹ is not part of the 2M scattering whose spectral weight dominated by a zone boundary magnon is limited below 200 cm⁻¹. As mentioned above, for extended Kitaev systems, non-LF scattering processes give rise to additional magnetic excitations [47]. In this light, the ME excitation comprises 2M-like excitations involving multiple exchange paths, multimagnon, or fractionalized excitations. We stress that the presence of residual fractionalized excitations is compatible with the $A_g(1)$ phonon anomalies [see Fig. 2(b)].

Next, we calculate the dynamic Raman susceptibility through the Kramers-Kronig relation $\chi^{\text{dyn}}(T) \equiv \frac{2}{\pi} \int_0^\infty \frac{\chi''(\omega, T)}{\omega} d\omega$ [52]. In Fig. 3(c), we plot the tempera-

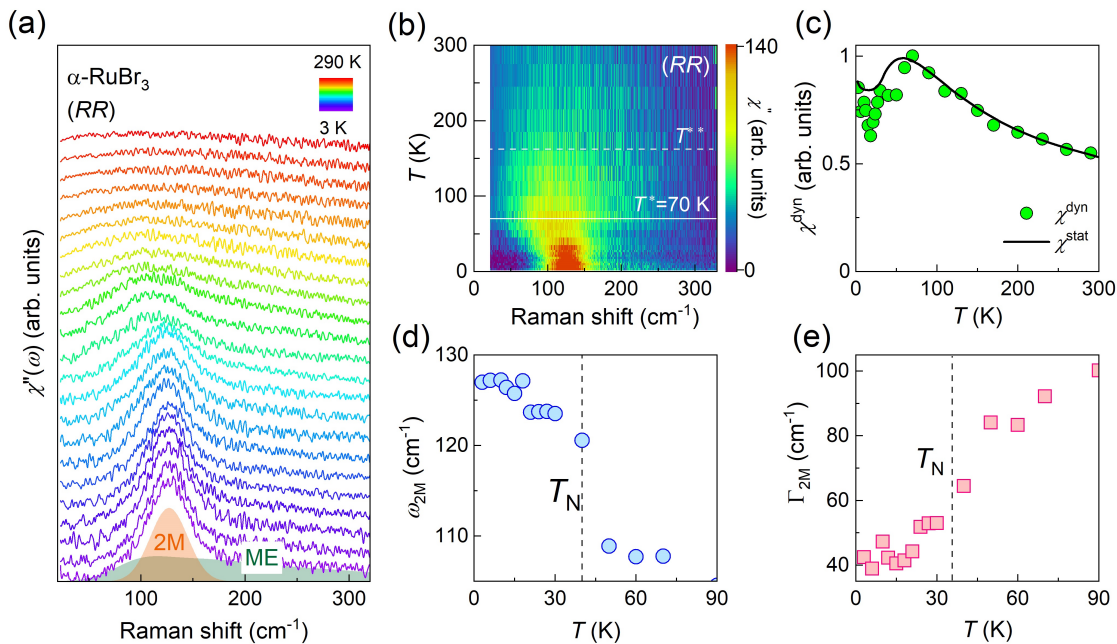


FIG. 3. (a) Temperature dependence of the magnetic Raman susceptibility $\chi''(\omega)$ of RuBr₃ obtained after subtracting phonon peaks in (RR) polarization. (b) Color plot of $\chi''(\omega)$ vs temperature. The solid and dashed lines mark the two characteristic temperatures T^* and T^{**} . (c) Temperature dependence of the dynamic Raman susceptibility plotted together with the static magnetic susceptibility. Temperature dependence of (d) the two-magnon peak energy ω_{2M} and (e) the linewidth Γ_{2M} . The vertical lines are the Néel temperature $T_N = 34$ K.

ture dependence of $\chi^{\text{dyn}}(T)$ together with the static susceptibility χ^{stat} measured by a SQUID magnetometer. $\chi^{\text{dyn}}(T)$ scales nicely with $\chi^{\text{stat}}(T)$. In a pure Kitaev system, the static and dynamic behavior are distinct from each other due to extremely short-ranged spin correlations. In this regard, the agreement between $\chi^{\text{dyn}}(T)$ and χ^{stat} signals the predominance of non-Kitaev magnetic correlations. In Figs. 3(d) and 3(e), we summarize the temperature dependence of the peak energy ω_{2M} and the linewidth Γ_{2M} of the 2M signal. We find that ω_{2M} and Γ_{2M} show notable changes as the temperature is increased through T_N . Further, we estimate the energy scale of exchange interactions from the 2M scattering. In the classical limit, the peak energy of the 2M continuum is given by $J(2zS - 1)$, where J is the exchange constant between the Ru spins, $z = 3$ is the number of NN spins, and $S = 1/2$ is the spin quantum number [37]. From $\omega_{2M} = 127 \text{ cm}^{-1}$, we obtain $J = 7.75 \text{ meV}$ ($\approx 90 \text{ K}$). The value J amounts to a sum of all exchange interactions including Kitaev, Heisenberg, Γ , and Γ' interactions.

Taken together, the temperature and polarization dependences of our magnetic Raman data evince that a dynamical response of RuBr₃ is largely governed by magnons. Further, we stress that the A_g symmetry of two-magnon excitations observed in RuBr₃ is distinct from the E_g symmetry of the fractionalized excitation in α -RuCl₃. Deviations from the conventional 2M behavior indicate that a small fraction of fractionalized excitations is also present. According to recent calculations by Kaib

et al. [29], the third NN Γ' term becomes stronger for RuBr₃. This along with enhanced interlayer interaction may be responsible for a more robust zigzag antiferromagnetic order, driving RuBr₃ to a classical limit.

D. Spin-orbit excitons

To shine a light on the Mott insulating $j_{\text{eff}} = 1/2$ state and the electronic structure, we measured electronic excitations at high-energy transfers up to 5000 cm^{-1} . In Fig. 4, we compare the high-energy Raman spectra between α -RuCl₃ and RuBr₃ at selected temperatures at $T = 3, 100,$ and 300 K . α -RuCl₃ and RuBr₃ commonly exhibit a double-peak feature at $A1 \approx 1986 \text{ cm}^{-1}$ and $A1' \approx 2294 \text{ cm}^{-1}$ and a single-peak excitation at $A2 \approx 3692 \text{ cm}^{-1}$.

The previous extensive studies of electronic structures of α -RuCl₃ [39, 53–55] established that the $A1$ and $A1'$ peaks correspond to a SO exciton that is excitonic quasiparticle excitations between the SOC-split levels $j_{\text{eff}} = 1/2$ and $j_{\text{eff}} = 3/2$. On the other hand, the $A2$ peak is assigned to a double SO exciton. The double-peak structure ($A1$ and $A1'$) is due to a trigonal distortion of RuX₆ octahedra, leading to the splitting of $j_{\text{eff}} = 3/2$ levels. Further, we note that a SO-entangled state is conditioned by SOC, Coulomb interaction, hopping integrals, and trigonal distortions. Given that the SOC increases with going from α -RuCl₃ to RuBr₃, it may appear counter-

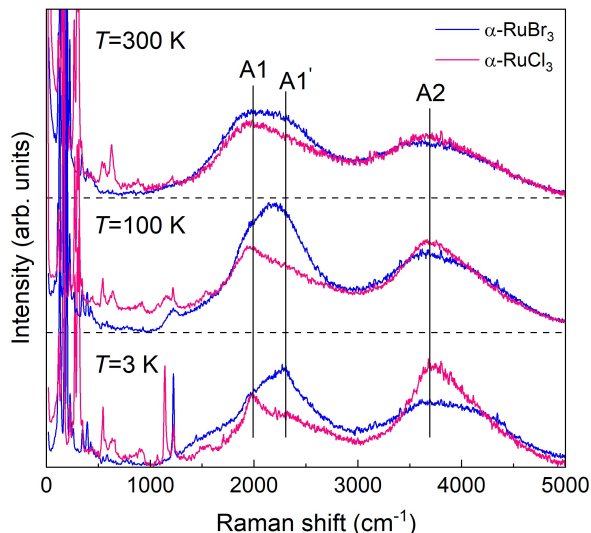


FIG. 4. Comparison of spin-orbit exciton excitations between α -RuCl₃ and RuBr₃ at selected temperatures at $T=300, 100,$ and 3 K. A1 and A1' denote the peaks of single spin-orbit exciton and A2 is the peak of double spin-orbit exciton.

intuitive that the SO-exciton energies hardly vary with the halogen atom X . On the qualitative level, the decrease of the hopping integrals with increasing X , which counteracts the increasing SOC, can explain why there is no essential difference of the SO excitons between RuX₃ ($X=Br, Cl$) [29].

Nonetheless, a close comparison reveals some discrepancies. At 3 K, the double SO exciton of RuBr₃ is suppressed relative to the single SO exciton. Unlike α -RuCl₃ that has the electronic bandgap of 1.1 eV, the reduced optical gap in RuBr₃ renders coupling between the SO exciton and charge excitations possible, leading to the damping of the double SO exciton. On heating, the double SO exciton dampens more rapidly than the single SO exciton due to the increase of thermally activated charge carriers, confirming our assertion. Our comparative study of SO excitons showcases that RuBr₃ realizes a SO entangled $j_{\text{eff}} = 1/2$ state to a similar degree as α -RuCl₃.

IV. CONCLUSIONS

To conclude, a comparative Raman scattering study of honeycomb polymorphs RuX₃ ($X=Cl, Br$) enables us to assess halogen-substitution effects on Kitaev magnetism and a spin-orbital-entangled $j_{\text{eff}} = 1/2$ state.

Our phonon data confirm a three-layer honeycomb lattice of RuBr₃, while lacking a structural phase transition unlike its counterpart α -RuCl₃. Both RuX₃ feature nearly identical single and double SO excitons in their energies and spectral forms, except that RuBr₃ is subject to charge fluctuations due to a reduced optical gap. This shows that a $j_{\text{eff}} = 1/2$ state is little affected by the stronger $p-d$ hybridization. The polarization and temperature dependence of magnetic excitations unveils that the symmetry and dynamics of a magnetic continuum are distinct between RuX₃. Based on the dominant scattering intensity in the A_g symmetry and the magnon-like thermal evolution of magnetic scattering, we infer that for RuBr₃, magnons occupy the majority of the magnetic spectral weight. This is contrasted by α -RuCl₃ whose magnetic scattering is dominated by E_g symmetry-allowed fractionalized excitations. Our results demonstrate that a halogen substitution in RuX₃ ($X=Cl, Br$) leads to a weakening of Kitaev magnetism possibly because the stronger $p-d$ hybridization enhances a third NN Γ' term against a NN Kitaev interaction. As such, further fine-tuning of exchange interactions by halogen engineering is needed for the ultimate stabilization of a Kitaev spin-liquid phase in the RuX₃ family.

ACKNOWLEDGMENTS

The work at SKKU was supported by the National Research Foundation (NRF) of Korea (Grants No. 2020R1A2C3012367 and No. 2020R1A5A1016518). The work at CAU was supported by NRF of Korea (Grants No. 2022R1A2C1003959 and No. 2020R1A5A1016518). D.W. acknowledges support from the Institute of Basic Science (IBS-R009-Y3). The work at Tohoku University is financially supported by JSPS KAKENHI (Nos. JP19H05823, JP19H05822, JP22H00102, and JP20H01850) and JST CREST (No. JP19198318). Y.I. thanks the financial support from JSPS KAKENHI (Nos. JP22K18680 and JP22H01175).

-
- [1] A. Kitaev, Anyons in an exactly solved model and beyond, *Annals of Physics* **321**, 2 (2006).
 [2] G. Jackeli and G. Khaliullin, Mott Insulators in the Strong Spin-Orbit Coupling Limit: From Heisenberg to a Quantum Compass and Kitaev Models, *Phys. Rev. Lett.* **102**, 017205 (2009).
 [3] Y. Singh and P. Gegenwart, Antiferromagnetic Mott insulating state in single crystals of the honeycomb lattice

- material Na₂IrO₃, *Phys. Rev. B* **82**, 064412 (2010).
 [4] K. W. Plumb, J. P. Clancy, L. J. Sandilands, V. V. Shankar, Y. F. Hu, K. S. Burch, H.-Y. Kee, and Y.-J. Kim, α -RuCl₃: A spin-orbit assisted Mott insulator on a honeycomb lattice, *Phys. Rev. B* **90**, 041112(R) (2014).
 [5] S. M. Winter, A. A. Tsirlin, M. Daghofer, J. van der Brink, Y. Singh, P. Gegenwart, and R. Valenti, Models and Materials for Generalized Kitaev Magnetism, *J.*

- Phys. Condens. Matter **29**, 493002 (2017).
- [6] M. Hermanns, I. Kimchi, and J. Knolle, Physics of the Kitaev model: Fractionalization, dynamic correlations, and material connections, *Annu. Rev. Condens. Matter Phys.* **9**, 17 (2018).
- [7] H. Takagi, T. Takayama, G. Jackeli, G. Khaliullin, and S. E. Nagler, Concept and realization of Kitaev quantum spin liquids, *Nat. Rev. Phys.* **1**, 264 (2019).
- [8] Y. Motome and J. Nasu, Hunting Majorana Fermions in Kitaev Magnets, *J. Phys. Soc. Jpn.* **89**, 012002 (2020).
- [9] S. Trebst and C. Hickey, Kitaev materials, *Physics Reports* **950**, 1 (2022).
- [10] J. Nasu, M. Udagawa, and Y. Motome, Vaporization of Kitaev Spin Liquids, *Phys. Rev. Lett.* **113**, 197205 (2014).
- [11] C. Hickey and S. Trebst, Emergence of a field-driven U(1) spin liquid in the Kitaev honeycomb model, *Nat. Commun.* **10**, 530 (2019).
- [12] H. G. von Schnering, K. Brodersen, F. Moers, H. K. Breitzbach, G. Thiele, Strukturuntersuchungen an β -RuCl₃, RuBr₃ und RuJ₃, *J. Common Met.* **11**, 288 (1966).
- [13] K. Brodersen, Structure of β -RuCl₃, RuI₃, IrBr₃, and IrI₃, *Angew. Chem. Int. Ed. Engl.* **7**, 148 (1968).
- [14] H. Hillebrecht, T. Ludwig, and G. Thiele, About trihalides with TiI₃ chain structure: Proof of pair forming of cations in β -RuCl₃ and RuBr₃ by temperature dependent single crystal x-ray analyses. *Z. Anorg. Allg. Chem.* **630**, 2199–2204 (2004).
- [15] C. Huang, J. Zhou, H. Wu, K. Deng, P. Jena, and E. Kan, Quantum anomalous Hall effect in ferromagnetic transition metal halides, *Phys. Rev. B* **95**, 045113 (2017).
- [16] F. Ersan, E. Vatansever, S. Sarikurt, Y. Yüksel, Y. Kadioglu, H. D. Ozaydin, O. Üzengi Aktürk, Ü. Akıncı, and E. Aktürk, Exploring the electronic and magnetic properties of new metal halides from bulk to two-dimensional monolayer: RuX₃ (X=Br,I), *J. Magn. Magn. Mater.* **476**, 111 (2019).
- [17] L. J. Sandilands, Y. Tian, K. W. Plumb, and Y.-J. Kim, Scattering Continuum and Possible Fractionalized Excitations in α -RuCl₃. *Phys. Rev. Lett.* **114**, 147201 (2014).
- [18] R. D. Johnson, S. C. Williams, A. A. Haghighirad, J. Singleton, V. Zapf, P. Manuel, I. I. Mazin, Y. Li, H. O. Jeschke, R. Valentí, and R. Coldea, Monoclinic crystal structure of α -RuCl₃ and the zigzag antiferromagnetic ground state. *Phys. Rev. B* **92**, 235119 (2015).
- [19] J. A. Sears, M. Songvilay, K. W. Plumb, J. P. Clancy, Y. Qiu, Y. Zhao, D. Parshall, and Y.-J. Kim, *Phys. Rev. B* **91**, 144420 (2015).
- [20] H.-S. Kim, and H.-Y. Kee, Crystal structure and magnetism in α -RuCl₃: an ab initio study, *Phys. Rev. B* **93**, 155143 (2016).
- [21] S.-H. Baek, S.-H. Do, K.-Y. Choi, Y. S. Kwon, A. U. B. Wolter, S. Nishimoto, J. van den Brink, and B. Büchner, Evidence for a Field-Induced Quantum Spin Liquid in α -RuCl₃, *Phys. Rev. Lett.* **119**, 037201 (2017).
- [22] A. Banerjee, J. Yan, J. Knolle, C. A. Bridges, M. B. Stone, M. D. Lumsden, D. G. Mandrus, D. A. Tennant, R. Moessner, and S. E. Nagler, Neutron scattering in the proximate quantum spin liquid α -RuCl₃, *Science* **356**, 1055–1059 (2017).
- [23] A. Glamazda, P. Lemmens, S.-H. Do, Y.S. Kwon, and K.-Y. Choi, Relation between Kitaev magnetism and structure in α -RuCl₃, *Phys. Rev. B* **95**, 174429 (2017).
- [24] S.-H. Do, S.-Y. Park, J. Yoshitake, J. Jasu, Y. Motome, Y. S. Kwon, D. T. Adroja, D. J. Voneshen, K. Kim, T.-H. Jang, J.-H. Park, K.-Y. Choi, S. Ji, Majorana fermions in the Kitaev quantum spin system α -RuCl₃, *Nat. Phys.* **13**, 1079 (2017).
- [25] Y. Imai, K. Nawa, Y. Shimizu, W. Yamada, H. Fujihara, T. Aoyama, R. Takahashi, D. Okuyama, T. Ohashi, M. Hagihala, S. Torii, D. Morikawa, M. Terauchi, T. Kawamata, M. Kato, H. Gotou, M. Itoh, T.J. Sato, and K. Ohgushi, Zigzag magnetic order in the Kitaev spin-liquid candidate material α -RuBr₃ with a honeycomb lattice, *Phys. Rev. B* **105**, L041112 (2022).
- [26] K. Nawa, Y. Imai, Y. Yamaji, H. Fujihara, W. Yamada, R. Takahashi, T. Hiraoka, M. Hagihala, S. Torii, T. Aoyama, T. Ohashi, Y. Shimizu, H. Gotou, M. I Itoh, K. Ohgushi, and T. J. Sato, Strongly electron-correlated semimetal RuI₃ with a layered honeycomb structure, *J. Phys. Soc. Jpn.* **90**, 123703 (2021).
- [27] D. Ni, X. Gui, K. M. Powderly, and R. J. Cava, Honeycomb-structure RuI₃, a new quantum material related to α -RuCl₃, *Adv. Mater.* **34**, 2106831 (2022).
- [28] H.-S. Kim, Spin-orbit-entangled nature of magnetic moments and Kitaev magnetism in layered halides, *Appl. Sci. Conver. Technol.* **30**, 191–194 (2021).
- [29] D. A. S. Kaib, K. Riedl, A. Razpopov, Y. Li, S. Backes, I. I. Mazin, and R. Valentí, Electronic and magnetic properties of the RuX₃ (X = Cl, Br, I) family: two siblings—and a cousin ? *npj Quantum Materials* **7**, 75 (2022).
- [30] Y. Zhang, L.-F. Lin, A. Moreo, and E. Dagotto, Theoretical study of the crystal and electronic properties of α -RuI₃, *Phys. Rev. B* **105**, 085107 (2022).
- [31] G. Li, X. Chen, Y. Gan, F. Li, M. Yan, F. Ye, S. Pei, Y. Zhang, L. Wang, H. Su, J. Dai, Y. Chen, Y. Shi, X. W. Wang, L. Zhang, S. Wang, D. Yu, F. Ye, J.-W. Mei, and M. Huang, Raman spectroscopy evidence for dimerization and Mott collapse in α -RuCl₃ under pressures, *Phys. Rev. Mater.* **3**, 023601 (2019).
- [32] T. T. Mai, A. McCreary, P. Lampen-Kelley, N. Butch, J. R. Simpson, J.-Q. Yan, S. E. Nagler, D. Mandrus, A. R. H. Walker, and R. V. Aguilar, Polarization-resolved Raman spectroscopy of α -RuCl₃ and evidence of room-temperature two-dimensional magnetic scattering, *Phys. Rev. B* **100**, 134419 (2019).
- [33] D. Lin, K. Ran, H. Zheng, J. Xu, L. Gao, J. Wen, S.-L. Yu, J.-X. Li, and X. Xi, Anisotropic scattering continuum induced by crystal symmetry reduction in atomically thin α -RuCl₃, *Phys. Rev. B* **101**, 045419 (2020).
- [34] A. Sahasrabudhe, D. A. S. Kaib, S. Reschke, R. German, T. C. Koethe, J. Buhot, D. Kamenskyi, C. Hickey, P. Becker, V. Tsurkan, A. Loidl, S. H. Do, K. Y. Choi, M. Grüninger, S. M. Winter, Zhe Wang, R. Valentí, and P. H. M. van Loosdrecht, High-field quantum disordered state in α -RuCl₃: Spin flips, bound states, and multiparticle continuum, *Phys. Rev. B* **101**, 140410(R) (2020).
- [35] D. Wulferding, Y. Choi, S.-H. Do, C. H. Lee, P. Lemmens, C. Faugeras, Y. Gallais, and K.-Y. Choi, Magnon bound states versus anionic Majorana excitations in the Kitaev honeycomb magnet α -RuCl₃, *Nat Commun* **11**, 1603 (2020).
- [36] S.-H. Do, C. H. Lee, T. Kihara, Y. S. Choi, S. Yoon, K. Kim, H. Cheong, W.-T. Chen, F. Chou, H. Nojiri, and K.-Y. Choi, Randomly Hopping Majorana Fermions in the Diluted Kitaev System α -Ru_{0.8}Ir_{0.2}Cl₃, *Phys. Rev. Lett.* **124**, 047204 (2020).

- [37] D. Wulferding, Y. Choi, W. Lee, and K.-Y. Choi, Raman spectroscopic diagnostic of quantum spin liquids, *J. Phys.: Condens. Matter* **32**, 043001 (2020).
- [38] Y. Wang, G. B. Osterhoudt, Y. Tian, P. Lampen-Kelley, A. Banerjee, T. Goldstein, J. Yan, J. Knolle, H. Ji, R. J. Cava, J. Nasu, Y. Motome, S. E. Nagler, D. Mandrus, and K. S. Burch, The range of non-Kitaev terms and fractional particles in α -RuCl₃, *npj Quantum Mater.* **5**, 14 (2020).
- [39] J.-H. Lee, Y. Choi, S.-H. Do, B. H. Kim, M.-J. Seong, and K.-Y. Choi, Multiple spin-orbit excitons in α -RuCl₃ from bulk to atomically thin layers, *npj Quantum Materials* **6**, 43 (2021).
- [40] A. Metavitsiadis, W. Natori, J. Knolle, and W. Brenig, Optical phonons coupled to a Kitaev spin liquid, *Phys. Rev. B* **105**, 165151 (2022).
- [41] K. Feng, S. Swarup, and N. B. Perkins, Footprints of Kitaev spin liquid in the Fano lineshape of Raman-active optical phonons, *Phys. Rev. B* **105**, L121108 (2022).
- [42] M. Ye, R. M. Fernandes, and N. B. Perkins, Phonon dynamics in the Kitaev spin liquid, *Phys. Rev. Resear.* **2**, 033180 (2020).
- [43] S.-Y. Park, S.-H. Do, K.-Y. Choi, D. Jang, T.-H. Jang, J. Schefer, C.-M. Wu, J. S. Gardner, M. S. Park, J.-H. Park, and Sungdae Ji, Emergence of the Isotropic Kitaev Honeycomb Lattice with Twodimensional Ising Universality in α -RuCl₃, arXiv:1609.05690 (2016).
- [44] D. P. Kozlenko, O. N. Lis, S. E. Kichanov, E. V. Lukin, N. M. Belozeroва, and B. N. Savenko, Spin-induced negative thermal expansion and spin-phonon coupling in van der Waals material CrCl₃, *npj Quantum Materials* **6**, 19 (2021).
- [45] M. Salavatib, N. Alajlana, Timon Rabczuk, Superstretchability in two-dimensional RuCl₃ and RuBr₃ confirmed by first-principles simulations, *Physica E: Low-dimensional Systems and Nanostructures* **113**, 79 (2019).
- [46] S. Yamamoto and T. Kimura, Raman Scattering Polarization and Single Spinon Identification in Two-Dimensional Kitaev Quantum Spin Liquids, *J. Phys. Soc. Jpn.* **89**, 063701 (2020).
- [47] Y. Yang, M. Li, I. Rousochatzakis, and N. B. Perkins, Non-Loudon-Fleury Raman scattering in spin-orbit coupled Mott insulators, *Phys. Rev. B* **104**, 144412 (2021).
- [48] M. Balkanski, R. F. Wallis, and E. Haro, Anharmonic effects in light scattering due to optical phonons in silicon, *Phys. Rev. B* **28**, 1928 (1928).
- [49] J. Nasu, J. Knolle, D. L. Kovrizhin, Y. Motome, and R. Moessner, Fermionic response from fractionalization in an insulating two-dimensional magnet, *Nat. Phys.* **12**, 912 (2016).
- [50] K.-Y. Choi, P. Lemmens, D. Heydhausen, G. Güntherodt, C. Baumann, R. Klingeler, P. Reutler, and B. Büchner, Anomalous orbital dynamics in LaSrMnO₄ observed by Raman spectroscopy, *Phys. Rev. B* **77**, 064415 (2008).
- [51] P. A. Fleury and R. Loudon, Scattering of Light by One- and Two- Magnon Excitations, *Phys. Rev.* **166**, 514 (1968).
- [52] *Frontiers in Solid State Sciences: Selected Topics in Magnetism*, edited by L. C. Gupta and M. S. Multani (World Scientific Singapore, 1993), Vol2.
- [53] Y. Hasegawa, T. Aoyama, K. Sasaki, Y. Ikemoto, T. Moriwaki, T. Shirakura, R. Saito, Y. Imai, and K. Ohgush, Two-phonon Absorption Spectra in the Layered Honeycomb Compound α -RuCl₃, *J. Phys. Soc. Jpn.* **86**, 123709 (2017).
- [54] B. W. Lebert, S. Kim, V. Bisogni, I. Jarrige, A. M. Barbour, and Y. J. Kim, Resonant inelastic x-ray scattering study of α -RuCl₃: a progress report, *J. Phys.:Condens. Matter* **32**, 144001 (2020).
- [55] P. Warzanowski, N. Borgwardt, K. Hopfer, J. Attig, T. C. Koethe, P. Becker, V. Tsurkan, A. Liodl, M. Hermanns, P. H. M. van Loosdrecht, and M. Grüninger, Multiple spin-orbit excitons and the electronic structure of α -RuCl₃, {*Phys. Rev. Resear.* **2**, 042007(R) (2020).